Published in final edited form as:

Clin Cancer Res. 2019 July 01; 25(13): 4117–4127. doi:10.1158/1078-0432.CCR-18-3224.

Targeted inhibition of the dual specificity phosphatases DUSP1 and DUSP6 suppress MPNST growth via JNK

Annmarie Ramkissoon[1], **Katherine E. Chaney**[1], **David Milewski**[1], **Kyle B. Williams**[2], **Rory L. Williams**[2], **Kwangmin Choi**[1], **Adam Miller**[3], **Tanya V. Kalin**[1], **Joseph G. Pressey**[1], **Sara Szabo**[1], **Mohammad Azam**[1], **David A. Largaespada**[2], and **Nancy Ratner**[1,3]

[1]Cincinnati Children's Hospital Medical Center,

[2]Masonic Cancer Center, University of Minnesota,

[3]University of Cincinnati College of Medicine.

Abstract

Purpose: In Neurofibromatosis Type 1 (NF1) and in highly aggressive malignant peripheral nerve sheath tumors (MPNSTs), constitutively active RAS-GTP and increased MAPK signaling are important in tumorigenesis. Dual specificity phosphatases (DUSPs) are negative regulators of MAPK signaling that dephosphorylate p38, JNK and ERK in different settings. While often acting as tumor suppressors, DUSPs may also act as oncogenes, helping tumor cells adapt to high levels of MAPK signaling. We hypothesized that inhibiting DUSPs might be selectively toxic to cells from NF1-driven tumors.

Experimental Design: We examined DUSPs gene and protein expression in neurofibroma and MPNST. We used shRNA to knockdown DUSP1 and 6 to evaluate cell growth, downstream MAPK signaling and mechanisms of action. We evaluated the DUSP inhibitor BCI in MPNST cell lines and in cell-line and patient-derived MPNST xenografts.

Results: DUSP1 and DUSP6 are expressed in NF1-deleted tumors. Knockdown of DUSP1 and DUSP6, alone or in combination, reduced MPNST cell growth and led to ERK and JNK-hyperactivation increasing downstream TP53 and p-ATM. The DUSP inhibitor BCI diminished survival of NF1-deleted Schwann cells and MPNST cell lines through activation of JNK. *In vivo*, treatment of an established cell-line xenograft or a novel patient-derived xenograft of MPNST with BCI increased ERK and JNK activation, caused tumor necrosis and fibrosis, and reduced tumor volume in one model.

Conclusions: Targeting DUSP1 and 6 genetically or with BCI effectively inhibits MPNST cell growth and promotes cell death, *in vitro* and in xenograft models. The data supports further investigation of DUSP inhibition in MPNST.

Keywords

MPNST; NF1; DUSP; MAPK; JNK

Corresponding Author: Nancy Ratner, Division of Experimental Hematology and Cancer Biology, Cincinnati Children's Hospital Medical Center, 3333 Burnet Avenue, ML. 7013, Cincinnati, OH 45229. Phone: 513-636-9469; Fax: 513-636-3549; Nancy.Ratner@cchmc.org.

INTRODUCTION

Malignant peripheral nerve sheath tumors (MPNST) are devastating chemotherapy and radiation resistant soft tissue sarcomas. Rare in the general population, half of MPNSTs arise in patients with the autosomal dominant genetic disorder called neurofibromatosis type 1 (NF1). MPNST in NF1 patients frequently occur in the context of pre-existing benign plexiform neurofibroma, and are the leading cause of death in adults with NF1 (1–3). *NF1* loss results in activation of RAS proteins that stimulates the MAPK family including ERK1 and ERK2, the c-Jun-N-terminal kinases (JNKs) 1, 2 and 3 and the p38 family of kinases (α, β, δ and γ) resulting in tumor cell growth. However, from gene expression microarray data, we and others have observed that key negative regulators of MAPK signaling are also increased in *NF1*-deleted tumors (4,5). Dual specificity phosphatase (DUSPs) expression is transcriptionally upregulated by increased ERK activity, providing a negative feedback loop to suppress RAS signaling (6). Within the DUSP family of proteins, the MAP kinase phosphatases (MKP) dephosphorylate tyrosine and serine/threonine residues on ERK, JNK and p38 (7). DUSPs are subdivided based on cellular localization and substrate specificity. There are over 10 members of this family including DUSP1/MKP-1, which is a nuclear MKP, and DUSP6/MKP-3, which is cytosolic (8). DUSPs substrate specificities depend on the cellular context (8).

Studies have described MAPK negative regulators, including DUSP6, as tumor suppressors. Thus, decreased expression of DUSP genes and proteins can occur in human cancer, including in tumors from pancreas and lung (9,10). In contrast, DUSPs are upregulated in some leukemia types including pre-B acute lymphoblastic leukemia (ALL) and DUSP1/6 inhibition has anti-tumor effects in gastric, breast and leukemia cancer models (11–14). In these cases, it is believed that DUSPs help tumors adapt to excessively high levels of growth factor signals. DUSP inhibition can acutely hyperactivate MAPK signaling, triggering activation of effectors such as p53, ATM and CHK½ that arrest cell growth and/or induce cell death. If *NF1*-deleted cells with RAS activation depend on DUSPs for growth and survival, then inhibiting DUSP could be effective in NF1 and in the many sporadic tumor types now known to show *NF1* loss (15).

Despite advances in understanding MPNST biology, there are no effective available MPNST treatments (2). Some potential targets are growth factor receptors, and the PI3K-AKT-mTOR and Wnt/β-catenin signaling pathways (16,17). Targeting MEK activity provides growth suppression in certain MPNST models, but effects, when present, are transient (5,18). Aurora kinase inhibition is cytostatic (19) and with combination therapy may show additive effects (20).

Targeting DUSP is an active area of preclinical development. BCI is a specific allosteric inhibitor of DUSP1 and 6 (12,13,21). Recently, in mouse models of leukemia and gastric cancer, BCI was effective in killing tumor cells *in vivo* (12–14,21). We hypothesized that inhibiting DUSPs might be selectively toxic to MPNST cells. In this study, we conducted molecular analyses to better understand the role of DUSP1 and DUSP6 in MPNST, using a combination of MPNST cell lines, i*n vivo* cell line xenografts and a novel patient derived

xenograft (PDX) MPNST model. The results from our studies demonstrate that DUSP1 and 6 protein expression are important for growth and survival in *NF1*-deleted MPNST and suggest that targeting DUSPs may be a therapeutic option for treating MPNST.

MATERIALS AND METHODS

Cell lines and drugs

Cell lines included immortalized human Schwann cells (iHSC) (22) with creation and characterization of NF1-deficient HSC1λ cell lines (Williams et al., unpublished). Briefly an early, common, exon of *NF1* (exon 10) was targeted to generate indel mutations using CRISPR/Cas9. Those found to be harboring homozygous frame shift mutations resulting in an early termination codon were considered *NF1* −/−. Cell lines showing homozygous wild-type (WT) sequences were considered isogenic WT controls. MPNST cell lines ST8814, S462.TY, STS26T and 90–8 were obtained as previously described (23,24). All MPNST cell lines were derived from NF1 patients, except STS26T. Cell lines were maintained in DMEM and 10% FBS and were confirmed negative for mycoplasma prior to use. Verification of cell lines was performed by Short Tandem Repeat (STR) DNA profiling (Genetica DNA Laboratories). Inhibitors used were (E)-2-benzylidene-3-(cyclohexylamino)-2,3-dihydro-1H-inden-1-one (BCI) (Axon Medchem), PD0325901 MEK inhibitor (gift from Kevin M. Shannon, UCSF), JNK inhibitors: JNK-IN-8 (Selleckchem) and SP600125 (LC Laboratories). Drugs were prepared as 10 mM stocks in DMSO and were diluted into media for cell culture treatments. Cell viability was quantified 72 hours after treatment by CellTiter 96® AQueous One Solution Cell Proliferation Assay (MTS) (Promega) as per manufacturer's instructions. Combination index data analysis was done using Calcusyn software (Version 1). Combination indices (CI) less than 0.9 indicate synergy, 0.9–1.1 indicate additivity, and greater than 1.1 indicate antagonism.

In vitro signaling experiments and TUNEL assays

Cells were serum starved for 16 hours in DMEM media (Life Technologies). MPNST cells were pre-treated with inhibitor for 15–60 mins then stimulated with DMEM and 10% FBS (Gemini Bio Products, CA) for 15–60 mins. The iHSCs were stimulated with DMEM-F12 with N2 supplement (Life Technologies) and 10 ng/mL beta Heregulin (b-HRG). Signaling experiments were terminated with a cold PBS wash, and cell lysates were generated for western blots. Cell death was analyzed with the In Situ Cell Death Detection Kit (TUNEL), TMR red (Roche), by fluorescence microscopy.

Western blotting

Tissues and cells were lysed in a RIPA buffer supplemented with protease and phosphatase inhibitors (Roche). Protein concentrations were determined with the BCA Protein Assay reagent (Thermo Fisher Scientific, Waltham). Antibodies used were Dusp1 (Millipore, 07–535), DUSP6 (Abcam, 76310), p38 (Abcam, 7925), p-p38 (Life 44684), p53 (Santa Cruz, sc-47698). Antibodies from Cell Signaling were p-DUSP-1 (2857), ERK, p-ERK (4695, 4370), JNK, p-JNK (9252, 4668), c-jun, p-c-jun (2315, 2361), p-p38 (9211), PARP (9542), Cyclin D1 (2922), p-ATM (13050), p-RB (retinoblastoma) (9301) and B-actin (5125). Blots were analyzed by densitometry using ImageJ software.

Knockdown experiments

For lentiviral shRNA infection, MPNST cells at 70% confluence were infected with lentiviral particles containing shRNAs targeting DUSP1 (TRCN0000002516, TRCN0000002517) or DUSP6 (TRCN0000002436, TRCN0000002437) at a MOI of 5. These were purchased from the Lenti-shRNA Library Core (Cincinnati Children's Hospital Medical Center; originally from the Sigma Mission Consortium shRNA library). pLKO.1-puro control was used as the non-targeting (NT) control. Cell lines were infected overnight in the presence of 10 μg/mL polybrene. Stable cell populations were selected with puromycin (2 μg/mL) 48 h later.

Quantitative PCR

Total RNA was isolated from cells using the RNeasy kit (Qiagen, Valencia, CA). The cDNA was made using the High Capacity cDNA Reverse Transcription Kit (Life Technologies). Real-time PCR was performed on cDNA using SYBR Green (Applied Biosystems). Relative quantification was performed using the ΔΔCT method, n=6.

Histological Staining

Formalin-fixed, paraffin-embedded tissue blocks were sectioned at 5 μm. Tissue sections were deparaffinized in xylene and rehydrated in ethanol, then water. Sections were stained with hematoxylin and eosin or Masson's trichrome, in which blue stain indicates collagen. For immunohistochemistry, sections were subjected to heat-induced antigen retrieval in citrate buffer. Sections were incubated with primary antibody overnight at 4°C and biotinylated secondary antibodies were detected with horseradish peroxidase-conjugated streptavidin (Elite ABC, Vector Laboratories) treated with DAB substrate (Vector Laboratories). Sections were counterstained with hematoxylin. The primary antibodies used for immunohistochemistry include anti-human nucleoli antibody (HNA) (Abcam, ab190710) and cleaved caspase 3 (CC3) (Cell signaling #9661).

Copy number alteration (CNA) data analysis

CNA data on 51 primary MPNSTs (NF1-associated and sporadic) was from a published GSE3388 data set (Agilent Human Genome CGH Microarray kit (4×44K)) (25). A circular binary segmentation (CBS) algorithm was applied to the log2 ratios of intensity values from tumor and normal to reduce local noise effects. CBS calculates a likelihood-ratio statistic for each array probe by permutation to locate change-points (26). After initial segmentation, smoothing, and post-segmentation normalization processes, CGHcall algorithm (27) was applied to assign each segment an aberration label. We chose the five-state (amplification, gain, normal, loss, and double-loss) prediction design and the probability of each state was calculated, then one state with the highest probability was chosen as a final CNA calling label for each segment.

Affymetrix GeneChip HU133 Plus 2.0 array for patient samples

We re-processed the published data (GEO accession #:GSE14038, Affymetrix GeneChip HU133 Plus 2.0) using Bioconductor's affy package (28). Differentially expressed genes between two groups were predicted using an adjusted t-test after multiple testing

(Benjamini-Hochberg) and Bioconductor's limma package (29). ANOVA test was performed using R (v3.3.1).

Mouse and xenograft tumor models

All animal studies were performed according to the guidelines of the Institutional Animal Care and Use Committee of Cincinnati Children's Hospital Medical Center (CCHMC). Mouse neurofibroma was obtained from *Nf1* fl/fl;Dhh-Cre mice as previously described (30). For the cell line-based xenograft model, S462.TY cells (1.25×10^6) in 30% Matrigel (BD Biosciences) were injected subcutaneously into the flank of 5- to 6-week-old female athymic nude mice. For the patient derived xenograft (PDX) MPNST model, biopsied tumor tissue was implanted subcutaneously directly into NOD.Cg-Prkdc^{scid} Il2rg^{tm1Wjl}/SzJ (NSG) mice. Tumors used for the study were grown in a donor mouse to a volume of approximately 2,500 mm^3. The tumor was harvested, cut into 1.5 mm^3 pieces and inserted subcutaneously into the flank of each mouse. Mice bearing F3–F4 grafts were used in this study. Drug dosing was started when tumors reached 150–200 mm^3. We measured tumors and weighed mice every three days. Tumor volume was calculated as follows: L × W2 (π/6), where L is the longest diameter and W is the width. The length of treatment was determined by the time tumors in each vehicle-treated group reached a maximum allowable tumor volume of 2500mm^3 (21 days for the PDX and 27 days for the S462.TY model).

Statistical analysis

Analyses were performed in GraphPad Prism software version 7.0. Data were mean +/− SD or SEM as indicated and was analyzed using ANOVA with Tukey's post hoc test or a Student's t-test, two-sided. P-values <0.05 were considered significant.

RESULTS

Expression of DUSP1 and DUSP6 in neurofibroma and MPNST

We used published gene expression profiles to analyze the differential expression of DUSP genes (5). DUSP1 and DUSP6 mRNAs were consistently elevated in neurofibroma and MPNST as compared to human Schwann cells, which is consistent with their transcriptional upregulation by mutant *NF1* (Fig. 1A). In a genetically engineered mouse model of neurofibroma, we examined DUSPs protein levels by immunoblot analysis. DUSP1 was 4x higher in neurofibroma compared to *Nf1*+/+ (wildtype) sciatic nerves (Fig. 1B). Anti-p-DUSP1 detects a phosphorylation site known to stabilize the protein (31); p-DUSP1 expression was elevated 7x (Fig. 1B). DUSP6 protein was 13x higher in neurofibroma compared to *Nf1*+/+ sciatic nerves (Fig. 1B). Compared to WT nerve, neurofibromas consistently showed elevated p-ERK, p-c-jun and decreased p-JNK, with variable levels of p-p38 (Supplementary Fig. S1A). In immortalized human Schwann cells (iHSC) lacking *NF1*, DUSP1 was 62% higher, p-DUSP1 2x and DUSP6 3x higher than isogenic wildtype iHSC (Fig. 1C), consistent with the idea that in Schwann cells, *NF1* deletion can drive increases in DUSP protein expression. DUSP protein was also elevated in human MPNST cell lines (n=4), showing an average 30% increase in DUSP1 and an average 3x higher expression of p-DUSP1 compared to iHSc (Fig. 1C). DUSP6 protein was 4–15x higher in MPNST compared to iHSC, with the highest expression in the *NF1*-deleted MPNST cell

line ST8814 (Fig.1C). Compared to iHSC, MPNST cells lines have increased p-ERK with variable levels of p-JNK and p-p38 (Supplementary Fig. S1B).

DUSP1 and *DUSP6* are on human chromosomes 5q35.1 and 12q21.33 respectively. Previous studies of MPNST have identified chromosomal gains in these regions (25,32). We reasoned that during the transformation process, some MPNSTs may genetically alter DUSPs to adapt to increased growth factor signaling. Amplifications of *HGF*, *MET*, and *PDGFRA* genes are present in some MPNSTs, suggesting a role in NF1 tumor progression (33). We analyzed data from human plexiform neurofibroma and primary MPNSTs (NF1-associated and sporadic) to evaluate the genomic status of *DUSP1* and *DUSP6* (25). We found no copy number changes in plexiform neurofibroma (Fig 1D). In NF1-associated MPNST, 31.25% of the tumors had copy number gains in *DUSP1* or *DUSP6*, with 12% having gains in both (Fig. 1D). In sporadic MPNSTs, 34% had gains in *DUSP1* or *DUSP6* with 5.7% having amplifications of *DUSP6* (Fig. 1D). Single copy loses of *DUSP1* or *DUSP6* were detected in 25% of NF1-associated MPNST with *DUSP1* or *DUSP6* loss at 8.6% and 5.7% in sporadic MPNST (Fig. 1D). Therefore, copy number changes is not likely be a major contributor to *DUSP1* or *6* expression in most MPNST.

DUSP1 and *DUSP6* knockdown decrease MPNST cell growth

We used shRNA to knockdown DUSP1 or DUSP6 in the MPNST cell line ST8814. Using two specific shRNAs and non-targeting (NT) controls, we validated DUSP1 or 6 knockdown of mRNA and a 55–75% decrease in protein (Fig. 2A–D). When DUSP1 was knocked down, levels of DUSP6 did not change and vice versa (Fig. 2C–D). Proliferation was decreased by 28–43% on DUSP1 knockdown and 40–51% on DUSP6 knockdown (Fig. 2E and F). DUSP1 knockdown cells treated with DUSP6 shRNA showed a further 30% decrease in proliferation (Fig. 2E). DUSP6 knockdown cells treated with DUSP1 shRNA showed a further 20% decrease in proliferation (Fig. 2F). Thus, directly decreasing DUSP1 or 6 levels, alone or in combination, decreases proliferation of MPNST cells.

DUSP1 and *DUSP6* knockdown activates ERK and JNK and regulates cell growth and death

We next tested the consequences of knockdown of DUSP1 or DUSP6 on MAPK signaling in the MPNST cell line ST8814. In DUSP1 knockdowns, 15 to 60 mins after serum stimulation, p-ERK and p-JNK were 1.75x higher compared to NT controls (Fig. 3A). The phosphorylated JNK substrate p-c-jun was 2x higher, and p-p38 was unchanged (Fig. 3A). In contrast, in DUSP6 knockdown ST8814 cells, p-ERK was only modestly increased (1.3x) (Fig. 3B). DUSP6 knockdown resulted in 2.58x higher p-JNK, and its substrate p-c-jun was 2x higher; p-p38 was unchanged compared to NT controls (Fig. 3B). DUSP1 knockdown cells treated with DUSP6 shRNA showed a 26% increase in p-ERK and larger increases in p-JNK and p-c-jun (71% and 56% respectively) compared to DUSP1 knockdown alone (Fig. 3C). Total protein levels of these markers were unchanged except for c-jun in DUSP6 knockdowns, which showed a modest increase (Supplementary Fig. S2A–C). We confirmed these results in the S462.TY MPNST cell line (Supplementary Fig. S2D and E). DUSP knockdown results in decreased proliferation and increased levels of p-ERK, p-JNK and p-c-

jun (Supplementary Fig. S2D and E). These data suggest that in MPNST cells DUSP1 and 6 play major roles in de-phosphorylation of MAPK.

We assessed the effect of DUSP1/6 downregulation on cell-cycle regulation and cell growth markers. Interestingly, upon DUSP1/6 silencing, cyclin D1 levels were reduced despite the high levels of MAPK signaling (Fig. 3D). Although sustained activation of ERK is required for cell cycle progression, hyperactivation of ERK or JNK signaling can lead to stabilization of p53 which can induce cell cycle arrest or cell death (34,35). Indeed, after knockdown of DUSP1, DUSP6 or both, p53 and p-ATM were increased, suggesting that this pathway is active in MPNST cells (Fig. 3D). In addition, knockdown of DUSP1 or DUSP6 induced a 64% increase in PARP cleavage and increased TUNEL+ cells compared to NT controls, indicating the induction of apoptotic cell death (Fig. 3D–E). Collectively, our results identify key pathways by which DUSPs are likely to regulate proliferation and cell death in MPNST cells.

DUSP inhibitor BCI reduces human MPNST cell growth and activates JNK

To verify these results, we tested the effect of the DUSP1/6 inhibitor BCI on the growth of the *NF1*-deleted MPNST cell lines ST8814 and S462.TY, and on *NF1*+/+ cell line iHSC-1λ and the sporadic MPNST cell line STS26T. We found that 2–4 uM BCI significantly inhibited MPNST cell growth 3 d after treatment (Fig. 4a). These concentrations were similarly effective in leukemia and gastric cancer cell lines (13,14). The iHSC-1λ and STS26T MPNST cell lines were less sensitive to BCI (Fig. 4a). We evaluated MAPK pathway activation by western blot analysis. Cells were serum starved overnight, incubated with 2 uM BCI then stimulated with serum-containing media. After 1 hr, p-ERK, p-JNK, p-c-jun and total c-jun were elevated in the BCI-treated MPNST cell lines ST8814 and S462.TY but did not change in iHSC-1λ (Fig. 4B and Supplementary Fig. S3A). There were no detectable differences in p-p38 (Fig. 4B). In contrast, in STS26T cells only p-p38 was increased and cyclin D1 decreased (Supplementary Fig. S3B). Within 24 hours, BCI decreased total PARP and increased cleaved PARP and CC3, indicative of apoptotic cell death in *NF1* deficient ST8814 and S462.TY cells (Fig. 4C). Also, there were 1.5–2x increases in TP53 and p-ATM in these BCI-treated cells correlating with reduced phospho-RB levels and reduced cell proliferation (Fig. 4C).

Given that blocking DUSPs, genetically or pharmacologically, increased p-JNK, we evaluated the possibility that JNK is a critical mediator of decreasing cell proliferation and/or increasing cell death, by testing if JNK inhibition would alter BCI effects in MPNSTs. In ST8814 MPNST cells treated with the irreversible JNK inhibitor JNK-IN-8 at 0.6–2.5 uM, cell proliferation was modestly increased (Supplementary Fig. S3C). These concentrations inhibit JNK activity as indicated by reduced p-c-jun (Supplementary Fig. S3D) (36). Targeting DUSP and JNK in combination reduced the effectiveness of BCI with combination indexes 1.2–3.9 indicating antagonism (Fig. 4D). Similar effects were seen with the JNK inhibitor SP600125 (Supplementary Fig. S3E and F). These data suggest that blocking DUSP phosphatase activity using BCI increases p-JNK causing effects on MPNST cells. Given that DUSP6 knockdown more effectively hyperactivates MAPKs in MPNST

ST8814 cells (Fig. 3B), our data suggest that BCI largely inhibits DUSP6 in *NF1*-deleted MPNST.

In MPNST cells, DUSP inhibition modestly increased phosphorylation of the MEK substrate ERK (Fig. 4B). We tested whether DUSP inhibition alters the effects of MEK inhibition in MPNST cell lines (Supplementary Fig. S4A and B). At 0.5–2 uM, BCI with 1.25 or 2.5 uM PD0325901, MEK inhibitory concentrations (5), there were no additive effects in ST8814 (CI 0.9) (Supplementary Fig. S4A and B) or STS26T (data not shown). In S462.TY, there was evidence of modest synergy (CI 0.29) over a narrow concentration range (Supplementary Fig. S4A and C). The effect of PD0325901 in combination with genetic knockdown of Dusp1 and 6 had no additive or antagonistic effect on cell proliferation (Supplementary Fig. S4D). Thus, DUSPs effects are mediated by JNK and combinations with MEKi may be modestly effective in some MPNST cell lines.

NF1 loss increases efficacy of BCI treatment

Since *NF1* deletion in iHSC increased DUSP1 and DUSP6 protein levels (Fig. 1C), we used these cell lines to determine whether BCI would inhibit proliferation in a *NF1*-dependent manner in Schwann cells. There was a therapeutic window in which *NF1*-deleted iHSCs were more susceptible compared to wildtype cells to the anti-proliferative effects of BCI (0.25–1 uM) (Fig. 5A). The largest difference was at 1 uM (Fig.5A). DUSP inhibition had lesser effects on iHSC *NF1* wildtype cells, in which the baseline activity of MAPK (p-ERK) was barely detectable (Fig. 5B). Consistent with direct inhibition of DUSPs with shRNA and with BCI in MPNST, 1 uM BCI enhanced p-ERK, p-JNK and p-c-jun signaling in *NF1*-deleted iHSC after 1 hr, (Fig. 5B and Supplementary Fig. S5A). Constitutive MAPK activity in the iHSC *NF1* −/− cells was strongly increased by treatment with BCI and correlated with increased levels of TP53 and p-ATM and reduced pRB and cyclin D1 (Fig. 5C). Evidence of cell death was variable, with evidence of cleaved PARP but not CC3, suggesting reduced proliferation as the predominate effect in these cells (Fig. 5C). As in MPNST cells, targeting DUSP and JNK in combination diminished the effectiveness of BCI in *NF1*−/− iHSC (CI>1.3) (Fig. 5D and Supplementary Fig. S5B). At these concentrations of JNK-IN-8, p-c-jun was reduced (Supplementary Fig. S5C). Thus, in *NF1* −/− Schwann cells and in MPNST cells with *NF1* deletion, DUSPs contributes to cell proliferation and survival. These data suggest that DUSPs act as oncogenes in this context.

In vivo effects of DUSP inhibitor BCI in MPNST xenograft models

We tested if BCI might be a useful therapeutic *in vivo* using an established cell line-based xenograft model, S462.TY MPNST cells (TY xenograft) engrafted subcutaneously into athymic nude mice. Tumor bearing mice were injected with BCI 10 mg/kg, i.p., once daily, 5x/wk for 27 days. No differences were detectable in tumor volume (Fig. 6A). In spite of the similar tumor volumes, excision of BCI-treated tumors revealed edema associated with encapsulated necrotic tissue that was absent in vehicle-treated mice; areas of necrosis ranged from 8–23% of section area (Fig. 6B and C).

We next used a novel PDX MPNST model which was developed by directly implanting patient tumor tissue into mice. The patient tumor had mutations in *NF1* and in other genes

common in human MPNST (*CDKN2A/B* loss and *SUZ12* mutation), *Rictor* was also amplified. The resulting xenograft MPNSTs maintained characteristics of the original tumor histologically (Supplementary Fig. S6A) and genetically with *NF1* and *SUZ12* mutations. Grafted tumors remained positive for human nucleoli antigen (HNA) (Supplementary Fig. S6B). BCI treatment at both doses significantly inhibited the growth of the PDX MPNSTs (Fig. 6D). In tissue sections, both the TY xenograft and the PDX MPNST model showed areas of cell apoptosis (CC3+ cells) and necrotic cell death on histology (TY 8–23%, PDX 2–17% vs VEH 1–2%) (Figures 6E, F). Both models also had areas of fibrosis/collagen deposits as indicated by trichrome staining (Supplementary Fig. S6C).

In the S462.TY xenograft, samples were collected on treatment day 27, 2 hours following the last BCI treatment, and analyzed for MAPK signaling and proliferation/cell death markers. BCI-treated tumors showed 60–90% increases in p-ERK, p-JNK and p-c-jun, 60% lower levels of cyclin D1 and variable levels of TP53 versus controls (Fig. 6G and Supplementary Fig. S6D and E). In the PDX model, after 21 d treatment, there was a trend toward MAPK activation (Supplementary Fig. S6F). Given that signaling data may be confounded by areas of necrosis and collagen/fibrosis, in the PDX model, signaling was analyzed after 12 days of BCI. These BCI-treated tumors had a significant 2.5–3.5X increased p-ERK, p-JNK and p-c-jun, 40% lower levels of cyclin D1 and a 46% increase in TP53 (Fig. 6H and Supplementary Fig. S6G and H). Upon discontinuing treatment in the PDX model, tumors showed regrowth and areas of proliferation among areas of necrosis and collagen deposits (Supplementary Fig. S7A). This suggests that BCI affects the MAPK pathway *in vivo* to transiently inhibit cell proliferation and induce cell death in MPNST.

Interestingly, in a separate study using the PDX model, we found that BCI (10mg/kg, i.p., 5X/wk) was as effective as the MEKi PD0325901 (1.5 mg/kg, 5X/wk) in inhibiting tumor growth (Supplementary Fig. S7B). We also tested PD0325901 (1.5 mg/kg, 5X/wk for 27 d), versus a combination of BCI and PD0325901 (10 mg/kg, 5X/wk for 27 d and 1.5 mg/kg, 5X/wk for 27 d respectively) in the TY xenograft model. As previously described, tumor volumes of MEK inhibitor-treated tumors were significantly lower compared to vehicle (Supplementary Fig. S7C). However, there was no significant tumor volume difference between the combination of BCI and PD0325901 versus PD0325901 only (Supplementary Fig. S7C). From histological analysis, BCI-treated tumors showed more necrotic cell death compared to MEK alone or treatment with the MEKi and DUSPi combination (Supplementary Fig. S7D). Areas of necrosis were also observed in the PDX xenograft model after BCI but not PD0325901 treatment (Supplementary Fig. S7D). Collectively, our data using two different *in vivo* xenograft MPNST models suggests that targeting DUSP1/6 with a single agent, BCI, suppresses MPNST growth and induces cell death.

DISCUSSION

Novel targets and treatment options for *NF1*-mediated MPNST are urgently needed. Dual specificity phosphatases regulate MAPK signaling by affecting diverse cellular processes including cell proliferation, cell survival and cell differentiation (37). We posited that understanding how DUSP family proteins affect *NF1*-mutant MPNST would suggest new approaches for MPNST therapy. Our analysis of DUSP1 and DUSP6 shows that both DUSP

proteins are overexpressed in MPNST compared to normal tissues under basal conditions, in cells and in growing tumors. DUSP1 and DUSP6 may have partially redundant functions in MPNST, and it is possible that other DUSPs, including DUSP22, also play roles. DUSP1 and 6 are up-regulated in *NF1*-mutant neurofibroma, iHSC and in MPNST cells. In these cell types DUSPs promote cell proliferation *in vitro*, as reducing levels of either or both, genetically or with the small molecule inhibitor BCI, decreases cell proliferation. DUSP1 and DUSP6 each also protect *NF1*-mutant MPNST cells from cell death, as silencing DUSP1 or DUSP6 in MPNST cells increased cell death *in vitro*. In two *in vivo* model systems, BCI, which specifically targets both DUSPs (12,21) caused necrotic and apoptotic cell death.

In most normal cells, DUSPs are transcriptionally upregulated in response to MAPK signaling, and function as negative feedback regulators to suppress RAS/MAPK signaling. DUSPs are often up-regulated in cancers harboring activating mutations in RAS or BRAF (6). The mechanisms underlying DUSP upregulation vary. Patients with pre-B ALL showed reduced CpG methylation of the *DUSP6* promoter as compared to normal pre-B cells (13). Gene amplification or increased transcription due to deletion of *NF1* and increased MAPK signaling may also play roles. In agreement with data from Courtois-Cox *et al.* (4), we find transcriptional up-regulation of DUSPs in *NF1* mutant cells. In addition, in 30% of MPNST the DUSP1 or DUSP6 locus, or both, are amplified.

Genetic knockdown of DUSP1 decreased tumorigenesis in orthotopic pancreatic tumors and in non-small-cell lung cancer (38,39). DUSP6 pro-survival effects were also described in chemoresistance screens, in glioblastoma cells and gastric cancer (14,40,41). The utility of the DUSP1/6 inhibitor BCI, or its analogs, as therapeutics remains to be tested. BCI is a small molecule identified in a zebrafish chemical screen that prevents catalytic phosphatase activity upon substrate binding, contributing to its specificity (21). An allosteric binding site for BCI exists within the phosphatase domains of both DUSP6 and DUSP1, but not in the related DUSP5; activity toward other DUSPs has not been excluded to date (12,21). BCI demonstrated single agent efficacy at doses 5–40 mg/kg, i.p daily (or twice daily) for up to one month in mouse models of gastric cancer and leukemia. These regimens effectively inhibited DUSP1/6 without noted toxicity, as did our doses within this range in MPNST xenografts (12–14). Inhibition of the MEK/ERK pathway combined with DUSP inhibition *in vivo* did not alter tumor volume or cell death when compared to single agents. Further studies may identify improved dosing regimens and schedules that maximize efficacy.

Previous work showed that inhibiting DUSPs can result in increased phosphorylation of ERK, JNK and/or p38 MAPKs (13). A predominant role for p-p38 was demonstrated in breast cancer and in therapy resistant chronic myeloid leukemia (CML) (11,12). In gastric cancer models, DUSP inhibition increased p-ERK, inducing cell death (14). In non-small-cell lung cancer, phosphorylated JNK and p38 affected tumor progression upon DUSP1 silencing (39). Indeed, recent DUSP6 KO studies failed to show expected effects on p-ERK; instead, p-JNK increased (42). These studies highlight the tumor specific MAPK substrate effects of DUSPs. In MPNST cells, DUSP knockdown or DUSP inhibition with BCI caused increased p-ERK, p-JNK and phosphorylation of the JNK substrate c-Jun. The finding that blocking JNK with either of two unrelated antagonists rescues the effects of BCI suggests

that in the *NF1*-deficient immortalized Schwann cells and MPNST cells we evaluated, DUSP1 and DUSP6 act largely on the JNK arm of the MAPK pathway, supporting the idea that JNK activation plays a critical role in BCI's anti-tumor effect in MPNST.

The duration of MAPK activation is controlled by cell expression of negative regulators of MAPK signaling, including GAPs, such as *NF1*, and phosphatases such as DUSPs (4). MAPK are known to inhibit growth and promote cell death through altering phosphorylation of RB and ATM, or through TP53 (43). Given that TP53, RB and ATM are central regulators of the cell cycle, the genetic status of these tumor suppressors may influence sensitivity to DUSP inhibitors. The incidence of mutation of TP53 is 40% in MPNST (44). In MPNST with wild-type TP53, DUSP inhibition with acute re-activation of JNK signaling appears to stabilize TP53, enabling the apoptotic pathway as occurs in other settings (34,35). In ovarian cancer cells, JNK promotes PARP phosphorylation leading to PARP degradation (45). Total and cleaved PARP play important roles in modulation of apoptosis and necrosis. Inhibition of DUSPs and PARP may induce DNA damage and prevent repair, potentially sensitizing radio-resistant MPNST cells to radiation therapy and cell death.

The S462.TY cell line model has a high tumorigenic potential in mice and so is widely used to evaluate therapies for MPNST. However, a single model cannot accurately represent the complexity and diversity of MPNST tumors. Models in which patient-derived tissues, including MPNST, are directly grafted into immunocompromised mice are increasingly used to test therapeutics (46). We describe a PDX model that contains common cancer-associated mutations found in patient MPNST: *NF1*, *CDKN2A/B*, *SUZ12* (47–49), and retains patient MPNST histological features. BCI treatment in this model slowed tumor growth and also promoted cell death. With BCI treatment, the differences in tumor volume between the models may have been due to edema, with a delay in clearance of the dying cells and collagen deposits that contribute to tumor volume. Such effects can confound analysis of drug effects on tumor volume, as shown after other drug treatments in sarcoma and xenografted tumors (50). Importantly, in both models, single agent BCI treatment was sufficient to cause cell death *in vivo*. For comparison, MEK inhibitor treatment transiently lowers tumor volumes, with no evidence of increased cell death (5).

In NF1-mediated transformation to MPNST, tumor cells appear to maintain MAPK activity within a narrow range to enable survival. DUSP inhibition, with increased MAPK signaling through JNK (and possibly other substrates), slows proliferation and can promote cell death. Our data support the development of agents targeting both DUSP1 and DUSP6 for NF1 patient MPNST.

Supplementary Material

Refer to Web version on PubMed Central for supplementary material.

ACKNOWLEDGMENTS

The authors thank Dr. Meenu Kesarwani for providing reagents and critical review of the manuscript, Dr. Tilat Rizvi for advice on immunohistochemistry, Jonathan Fletcher for tumor dissection assistance and Kierra Ware for immunoblot assistance.

Financial support:

This work was supported by R01 NS086219 (to DL and NR), a grant from the Children's Tumor Foundation-Synodos (to DL), and CancerFree KIDS grants (to AR). AM was supported by a summer fellowship (NIH T35DK060444).

REFERENCES

1. Ducatman BS, Scheithauer BW, Piepgras DG, Reiman HM, Ilstrup DM. Malignant peripheral nerve sheath tumors. A clinicopathologic study of 120 cases. Cancer 1986;57(10):2006–21. [PubMed: 3082508]
2. Kim A, Stewart DR, Reilly KM, Viskochil D, Miettinen MM, Widemann BC. Malignant Peripheral Nerve Sheath Tumors State of the Science: Leveraging Clinical and Biological Insights into Effective Therapies. Sarcoma 2017;2017:7429697. [PubMed: 28592921]
3. Uusitalo E, Rantanen M, Kallionpaa RA, Poyhonen M, Leppavirta J, Yla-Outinen H, et al. Distinctive Cancer Associations in Patients With Neurofibromatosis Type 1. J Clin Oncol 2016;34(17):1978–86. [PubMed: 26926675]
4. Courtois-Cox S, Genther Williams SM, Reczek EE, Johnson BW, McGillicuddy LT, Johannessen CM, et al. A negative feedback signaling network underlies oncogene-induced senescence. Cancer Cell 2006;10(6):459–72. [PubMed: 17157787]
5. Jessen WJ, Miller SJ, Jousma E, Wu J, Rizvi TA, Brundage ME, et al. MEK inhibition exhibits efficacy in human and mouse neurofibromatosis tumors. J Clin Invest 2013;123(1):340–7. [PubMed: 23221341]
6. Pratilas CA, Taylor BS, Ye Q, Viale A, Sander C, Solit DB, et al. (V600E)BRAF is associated with disabled feedback inhibition of RAF-MEK signaling and elevated transcriptional output of the pathway. Proc Natl Acad Sci U S A 2009;106(11):4519–24. [PubMed: 19251651]
7. Caunt CJ, Keyse SM. Dual-specificity MAP kinase phosphatases (MKPs): shaping the outcome of MAP kinase signalling. FEBS J 2013;280(2):489–504. [PubMed: 22812510]
8. Patterson KI, Brummer T, O'Brien PM, Daly RJ. Dual-specificity phosphatases: critical regulators with diverse cellular targets. Biochem J 2009;418(3):475–89. [PubMed: 19228121]
9. Furukawa T, Sunamura M, Motoi F, Matsuno S, Horii A. Potential tumor suppressive pathway involving DUSP6/MKP-3 in pancreatic cancer. Am J Pathol 2003;162(6):1807–15. [PubMed: 12759238]
10. Okudela K, Yazawa T, Woo T, Sakaeda M, Ishii J, Mitsui H, et al. Down-regulation of DUSP6 expression in lung cancer: its mechanism and potential role in carcinogenesis. Am J Pathol 2009;175(2):867–81. [PubMed: 19608870]
11. Kaltenmeier CT, Vollmer LL, Vernetti LA, Caprio L, Davis K, Korotchenko VN, et al. A Tumor Cell-Selective Inhibitor of Mitogen-Activated Protein Kinase Phosphatases Sensitizes Breast Cancer Cells to Lymphokine-Activated Killer Cell Activity. J Pharmacol Exp Ther 2017;361(1): 39–50. [PubMed: 28154014]
12. Kesarwani M, Kincaid Z, Gomaa A, Huber E, Rohrabaugh S, Siddiqui Z, et al. Targeting c-FOS and DUSP1 abrogates intrinsic resistance to tyrosine-kinase inhibitor therapy in BCR-ABL-induced leukemia. Nat Med 2017;23(4):472–82. [PubMed: 28319094]
13. Shojaee S, Caeser R, Buchner M, Park E, Swaminathan S, Hurtz C, et al. Erk Negative Feedback Control Enables Pre-B Cell Transformation and Represents a Therapeutic Target in Acute Lymphoblastic Leukemia. Cancer Cell 2015;28(1):114–28. [PubMed: 26073130]
14. Wu QN, Liao YF, Lu YX, Wang Y, Lu JH, Zeng ZL, et al. Pharmacological inhibition of DUSP6 suppresses gastric cancer growth and metastasis and overcomes cisplatin resistance. Cancer Lett 2018;412:243–55. [PubMed: 29050982]
15. Philpott C, Tovell H, Frayling IM, Cooper DN, Upadhyaya M. The NF1 somatic mutational landscape in sporadic human cancers. Hum Genomics 2017;11(1):13. [PubMed: 28637487]
16. Patwardhan PP, Surriga O, Beckman MJ, de Stanchina E, Dematteo RP, Tap WD, et al. Sustained inhibition of receptor tyrosine kinases and macrophage depletion by PLX3397 and rapamycin as a potential new approach for the treatment of MPNSTs. Clin Cancer Res 2014;20(12):3146–58. [PubMed: 24718867]

17. Rahrmann EP, Watson AL, Keng VW, Choi K, Moriarity BS, Beckmann DA, et al. Forward genetic screen for malignant peripheral nerve sheath tumor formation identifies new genes and pathways driving tumorigenesis. Nat Genet 2013;45(7):756–66. [PubMed: 23685747]
18. Dodd RD, Mito JK, Eward WC, Chitalia R, Sachdeva M, Ma Y, et al. NF1 deletion generates multiple subtypes of soft-tissue sarcoma that respond to MEK inhibition. Mol Cancer Ther 2013;12(9):1906–17. [PubMed: 23858101]
19. Patel AV, Eaves D, Jessen WJ, Rizvi TA, Ecsedy JA, Qian MG, et al. Ras-driven transcriptome analysis identifies aurora kinase A as a potential malignant peripheral nerve sheath tumor therapeutic target. Clin Cancer Res 2012;18(18):5020–30. [PubMed: 22811580]
20. Currier MA, Sprague L, Rizvi TA, Nartker B, Chen CY, Wang PY, et al. Aurora A kinase inhibition enhances oncolytic herpes virotherapy through cytotoxic synergy and innate cellular immune modulation. Oncotarget 2017;8(11):17412–27. [PubMed: 28147331]
21. Molina G, Vogt A, Bakan A, Dai W, Queiroz de Oliveira P, Znosko W, et al. Zebrafish chemical screening reveals an inhibitor of Dusp6 that expands cardiac cell lineages. Nat Chem Biol 2009;5(9):680–7. [PubMed: 19578332]
22. Li H, Chang LJ, Neubauer DR, Muir DF, Wallace MR. Immortalization of human normal and NF1 neurofibroma Schwann cells. Lab Invest 2016;96(10):1105–15. [PubMed: 27617404]
23. DeClue JE, Papageorge AG, Fletcher JA, Diehl SR, Ratner N, Vass WC, et al. Abnormal regulation of mammalian p21ras contributes to malignant tumor growth in von Recklinghausen (type 1) neurofibromatosis. Cell 1992;69(2):265–73. [PubMed: 1568246]
24. Miller SJ, Rangwala F, Williams J, Ackerman P, Kong S, Jegga AG, et al. Large-scale molecular comparison of human schwann cells to malignant peripheral nerve sheath tumor cell lines and tissues. Cancer Res 2006;66(5):2584–91. [PubMed: 16510576]
25. Yang J, Ylipaa A, Sun Y, Zheng H, Chen K, Nykter M, et al. Genomic and molecular characterization of malignant peripheral nerve sheath tumor identifies the IGF1R pathway as a primary target for treatment. Clin Cancer Res 2011;17(24):7563–73. [PubMed: 22042973]
26. Olshen AB, Venkatraman ES, Lucito R, Wigler M. Circular binary segmentation for the analysis of array-based DNA copy number data. Biostatistics 2004;5(4):557–72. [PubMed: 15475419]
27. van de Wiel MA, Kim KI, Vosse SJ, van Wieringen WN, Wilting SM, Ylstra B. CGHcall: calling aberrations for array CGH tumor profiles. Bioinformatics 2007;23(7):892–4. [PubMed: 17267432]
28. Gautier L, Cope L, Bolstad BM, Irizarry RA. affy--analysis of Affymetrix GeneChip data at the probe level. Bioinformatics 2004;20(3):307–15. [PubMed: 14960456]
29. Ritchie ME, Phipson B, Wu D, Hu Y, Law CW, Shi W, et al. limma powers differential expression analyses for RNA-sequencing and microarray studies. Nucleic Acids Res 2015;43(7):e47. [PubMed: 25605792]
30. Wu J, Williams JP, Rizvi TA, Kordich JJ, Witte D, Meijer D, et al. Plexiform and dermal neurofibromas and pigmentation are caused by Nf1 loss in desert hedgehog-expressing cells. Cancer Cell 2008;13(2):105–16. [PubMed: 18242511]
31. Brondello JM, Pouyssegur J, McKenzie FR. Reduced MAP kinase phosphatase-1 degradation after p42/p44MAPK-dependent phosphorylation. Science 1999;286(5449):2514–7. [PubMed: 10617468]
32. Schmidt H, Taubert H, Meye A, Wurl P, Bache M, Bartel F, et al. Gains in chromosomes 7, 8q, 15q and 17q are characteristic changes in malignant but not in benign peripheral nerve sheath tumors from patients with Recklinghausen's disease. Cancer Lett 2000;155(2):181–90. [PubMed: 10822134]
33. Mantripragada KK, Spurlock G, Kluwe L, Chuzhanova N, Ferner RE, Frayling IM, et al. High-resolution DNA copy number profiling of malignant peripheral nerve sheath tumors using targeted microarray-based comparative genomic hybridization. Clin Cancer Res 2008;14(4):1015–24. [PubMed: 18281533]
34. Fuchs SY, Adler V, Pincus MR, Ronai Z. MEKK1/JNK signaling stabilizes and activates p53. Proc Natl Acad Sci U S A 1998;95(18):10541–6. [PubMed: 9724739]
35. Golding SE, Rosenberg E, Neill S, Dent P, Povirk LF, Valerie K. Extracellular signal-related kinase positively regulates ataxia telangiectasia mutated, homologous recombination repair, and the DNA damage response. Cancer Res 2007;67(3):1046–53. [PubMed: 17283137]

36. Xie X, Kaoud TS, Edupuganti R, Zhang T, Kogawa T, Zhao Y, et al. c-Jun N-terminal kinase promotes stem cell phenotype in triple-negative breast cancer through upregulation of Notch1 via activation of c-Jun. Oncogene 2017;36(18):2599–608. [PubMed: 27941886]
37. Kidger AM, Keyse SM. The regulation of oncogenic Ras/ERK signalling by dual-specificity mitogen activated protein kinase phosphatases (MKPs). Semin Cell Dev Biol 2016;50:125–32. [PubMed: 26791049]
38. Liu F, Gore AJ, Wilson JL, Korc M. DUSP1 is a novel target for enhancing pancreatic cancer cell sensitivity to gemcitabine. PLoS One 2014;9(1):e84982. [PubMed: 24409315]
39. Moncho-Amor V, Ibanez de Caceres I, Bandres E, Martinez-Poveda B, Orgaz JL, Sanchez-Perez I, et al. DUSP1/MKP1 promotes angiogenesis, invasion and metastasis in non-small-cell lung cancer. Oncogene 2011;30(6):668–78. [PubMed: 20890299]
40. MacKeigan JP, Murphy LO, Blenis J. Sensitized RNAi screen of human kinases and phosphatases identifies new regulators of apoptosis and chemoresistance. Nat Cell Biol 2005;7(6):591–600. [PubMed: 15864305]
41. Messina S, Frati L, Leonetti C, Zuchegna C, Di Zazzo E, Calogero A, et al. Dual-specificity phosphatase DUSP6 has tumor-promoting properties in human glioblastomas. Oncogene 2011;30(35):3813–20. [PubMed: 21499306]
42. Hsu WC, Chen MY, Hsu SC, Huang LR, Kao CY, Cheng WH, et al. DUSP6 mediates T cell receptor-engaged glycolysis and restrains TFH cell differentiation. Proc Natl Acad Sci U S A 2018;115(34):E8027–E36. [PubMed: 30087184]
43. Wada T, Penninger JM. Mitogen-activated protein kinases in apoptosis regulation. Oncogene 2004;23(16):2838–49. [PubMed: 15077147]
44. Brohl AS, Kahen E, Yoder SJ, Teer JK, Reed DR. The genomic landscape of malignant peripheral nerve sheath tumors: diverse drivers of Ras pathway activation. Sci Rep 2017;7(1):14992. [PubMed: 29118384]
45. Wang J, Kho DH, Zhou JY, Davis RJ, Wu GS. MKP-1 suppresses PARP-1 degradation to mediate cisplatin resistance. Oncogene 2017;36(43):5939–47. [PubMed: 28650468]
46. Castellsague J, Gel B, Fernandez-Rodriguez J, Llatjos R, Blanco I, Benavente Y, et al. Comprehensive establishment and characterization of orthoxenograft mouse models of malignant peripheral nerve sheath tumors for personalized medicine. EMBO Mol Med 2015;7(5):608–27. [PubMed: 25810463]
47. Birindelli S, Perrone F, Oggionni M, Lavarino C, Pasini B, Vergani B, et al. Rb and TP53 pathway alterations in sporadic and NF1-related malignant peripheral nerve sheath tumors. Lab Invest 2001;81(6):833–44. [PubMed: 11406645]
48. De Raedt T, Beert E, Pasmant E, Luscan A, Brems H, Ortonne N, et al. PRC2 loss amplifies Ras-driven transcription and confers sensitivity to BRD4-based therapies. Nature 2014;514(7521):247–51. [PubMed: 25119042]
49. Lee W, Teckie S, Wiesner T, Ran L, Prieto Granada CN, Lin M, et al. PRC2 is recurrently inactivated through EED or SUZ12 loss in malignant peripheral nerve sheath tumors. Nat Genet 2014;46(11):1227–32. [PubMed: 25240281]
50. Ran L, Chen Y, Sher J, Wong EWP, Murphy D, Zhang JQ, et al. FOXF1 Defines the Core-Regulatory Circuitry in Gastrointestinal Stromal Tumor. Cancer Discov 2018;8(2):234–51. [PubMed: 29162563]

TRANSLATIONAL RELEVANCE

Malignant peripheral nerve sheath tumors (MPNST) are devastating, therapy resistant, tumors. Preclinical inhibition of MAPK signaling suppresses tumor growth, but the effects are transient. DUSPs are upregulated in response to elevated MAPK signaling in cancer cells with NF1 deletion, restraining signaling and helping cells to adapt to oncogenic signals. Here, we demonstrate that neurofibroma and MPNST express DUSP1 and DUSP6, and that genetic blockade of these targets inhibits the growth of MPNST cells *in vitro*. This occurs largely through activation of JNK, which affects p53 and RB, triggering growth arrest and/or cell death. Furthermore, in mice with orthotopic human MPNST xenografts, the DUSP1/6 inhibitor BCI induces cell death and increases fibrosis in two xenograft models, resulting in decreased tumor volume in one model. Our preclinical work supports the development of DUSP1/6 inhibitors for MPNST therapy.

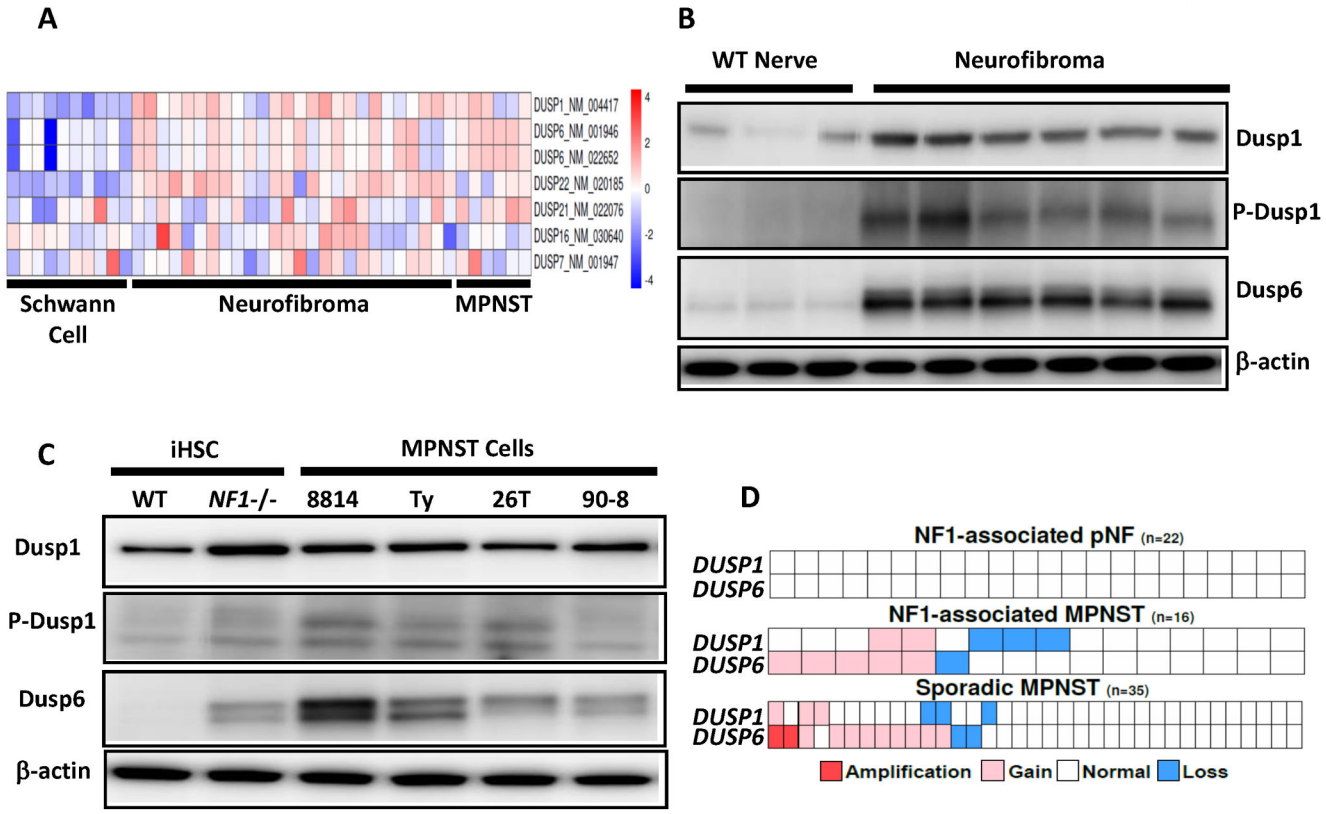

Figure 1.

Expression of DUSP1 and DUSP6 in neurofibroma and MPNST. **A**, Gene expression microarray showing DUSP transcripts with increased expression in plexiform neurofibroma tumors and MPNST solid tumors versus normal human Schwann cells. The scale bar on right shows mean log2-transformed normalized fold change. **B**, Immunoblot shows elevated DUSP1, p-DUSP1 and DUSP6 protein in Dhh Cre; *Nf1* fl/fl mouse neurofibroma versus normal age-matched wildtype sciatic nerve (WT nerve). **C**, Immunoblot shows elevated DUSP, p-DUSP1 and DUSP6 protein in *NF1*−/− iHSC and MPNST cell lines versus *NF1* WT iHSC. β-actin was used as a loading control. **D**, Copy number alteration (CNA) data analysis of plexiform neurofibroma (pNF), NF1-associated MPNST and sporadic MPNST.

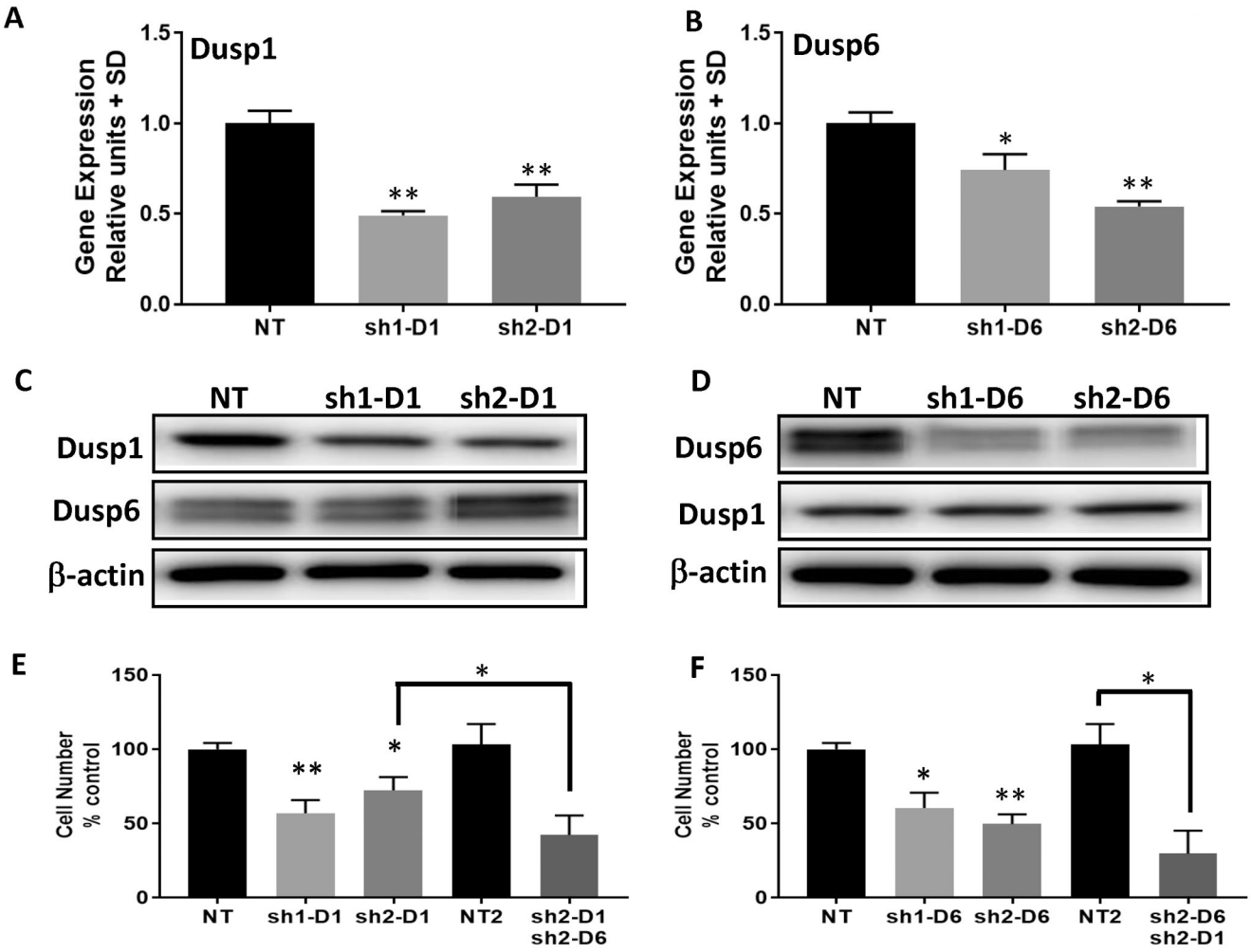

Figure 2.

DUSP1 and DUSP6 knockdown decrease cell growth in the *NF1*−/− MPNST cell line ST8814. **A** and **B**, mRNA expression levels in the MPNST cell line ST8814 after lentiviral shRNA knockdown of DUSP1 or DUSP6. Levels are expressed as normalized to non-targeting (NT) shRNA controls. (*) and (**) represents P<0.05 and P<0.01 compared to NT control. **C**, Immunoblots show that DUSP1 protein expression, but not DUSP6, is reduced by day 4 post transduction with two DUSP1 shRNAs **D**, DUSP6 protein expression, but not DUSP1, is reduced by day 4 post transduction with two DUSP6 shRNAs. **E**, shDUSP1 reduces cell proliferation alone and in combination with sh2-DUSP6. **F**, shDUSP6 reduces cell proliferation alone and in combination with sh2-DUSP1. (*) and (**) represent P<0.05 and P<0.01 compared to NT control. Experiments were done twice with n=6 per experiment.

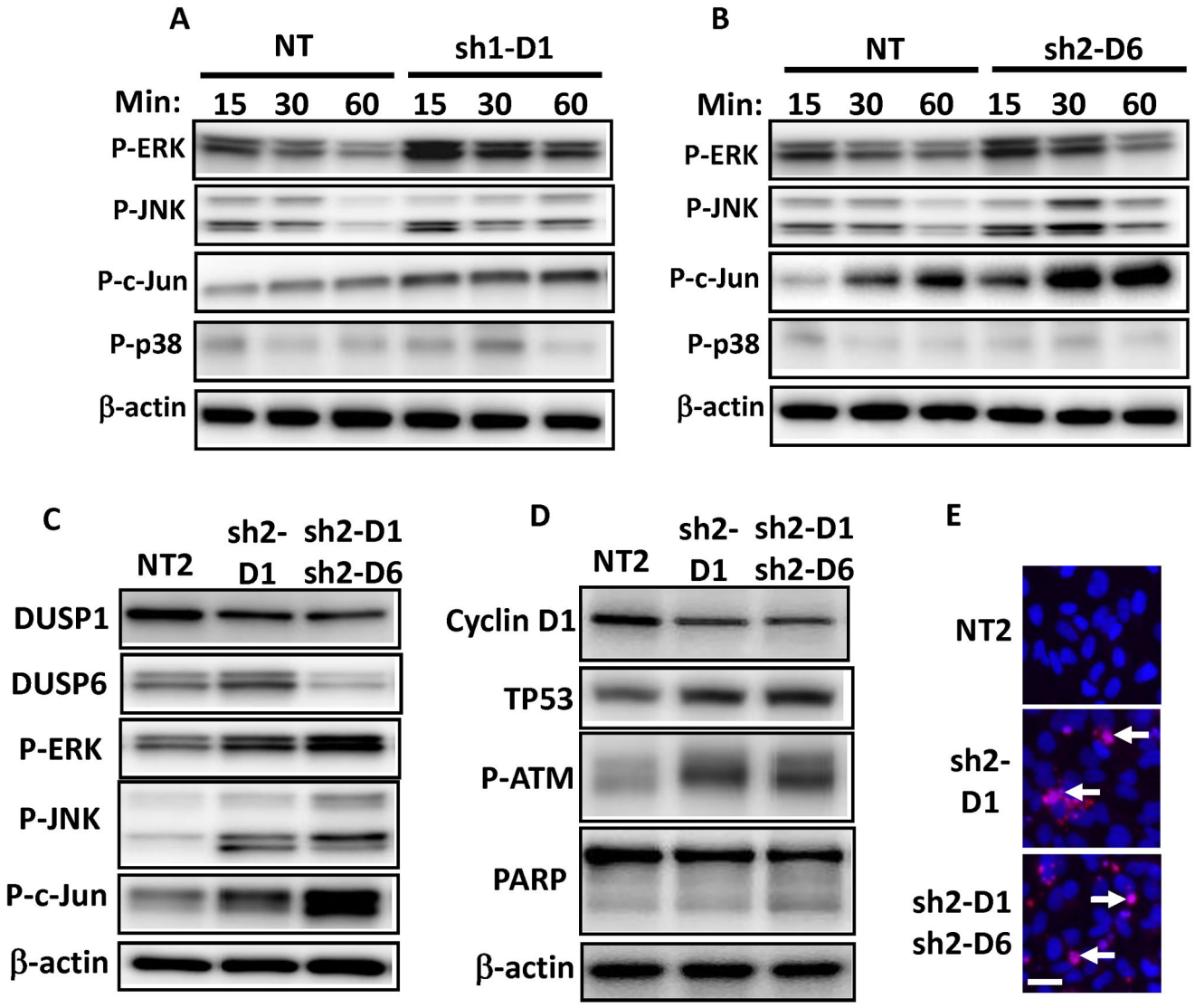

Figure 3.

Activation of ERK and JNK in the *NF1*−/− MPNST cell line ST8814 by shDUSP1 and shDUSP6 knockdown. **A**, ST8814 MPNST cells infected with shRNA targeting DUSP1 (sh1–D1) or **B**, shRNA targeting DUSP6 (sh2–D6) were starved overnight in media without serum. Cells were then stimulated with DMEM and 10% FBS for designated minutes (min). Immunoblots were analyzed for p-ERK, p-JNK, p-c-jun and p-p38 with β-actin as a loading control. **C**, MAPK signaling effects of DUSP1 shRNA-2 (sh2–D1) alone or in combination with DUSP6 shRNA2 (sh2–D6) in ST8814. **D**, Immunoblot analysis of TP53, p-ATM, cyclin D1 and PARP in ST8814 cells infected with DUSP1 shRNA-2 (sh2–D1) alone and in combination with DUSP6 shRNA2 (sh2–D6). Immunoblots were quantified by densitometry and expressed as percentages relative to NT2 controls (see text). **E**, Cell death analyzed with TUNEL fluorescence microscopy (red signal) with nuclei stained with DAPI (blue signal). Arrows indicate dying cells. Scale bar is 25 um.

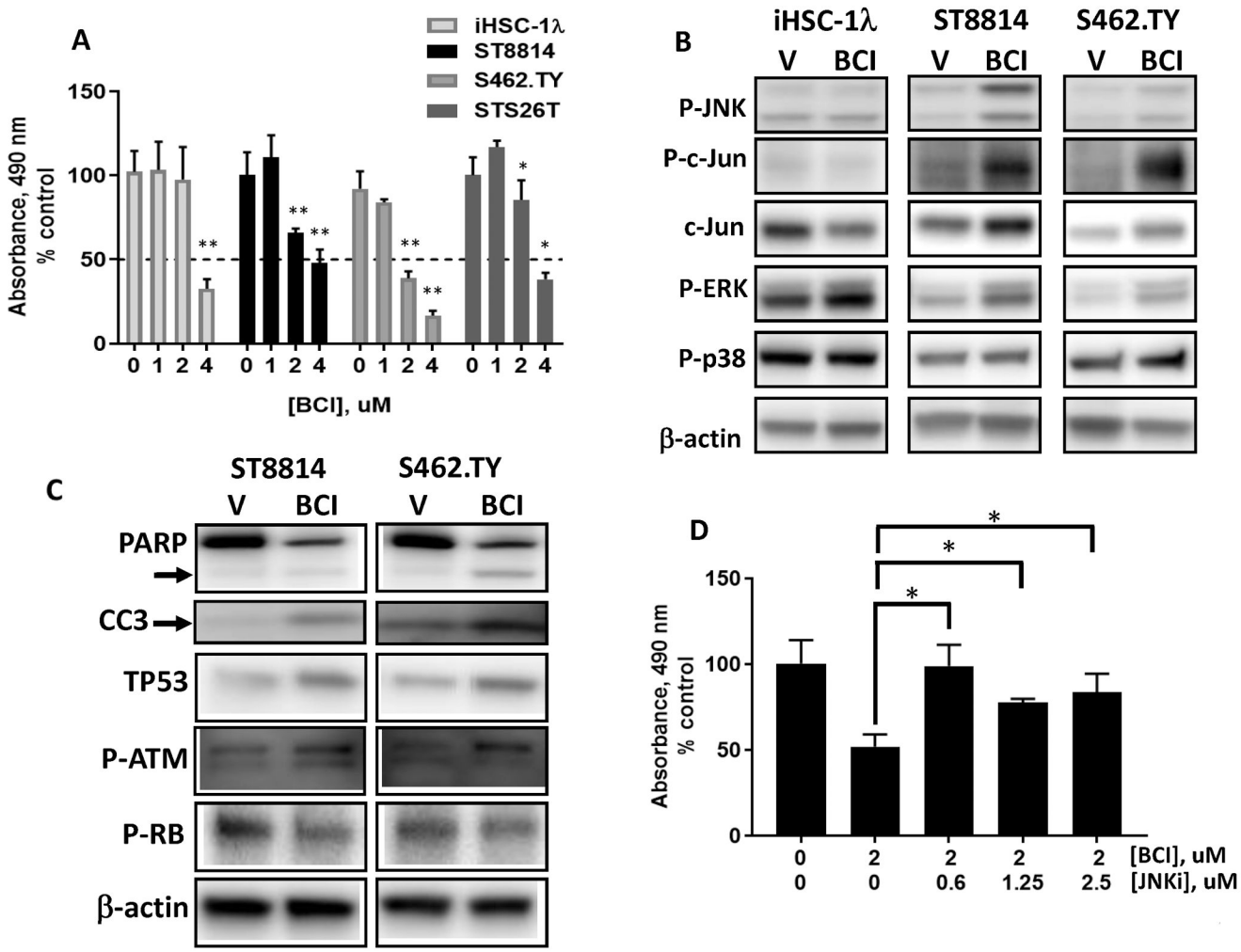

Figure 4.

The DUSP inhibitor BCI suppresses human MPNST cell growth via JNK activation. **A**, Cell survival was measured with the MTS assay (OD at 490 nm) after 3 days. Cells were serum starved overnight then treated with BCI in DMEM and 10% FBS. **B**, Immunoblot analysis of MAPK signaling. MPNST cells were starved overnight, incubated with BCI (2 uM) for 60 mins then stimulated with DMEM and 10% FBS for 1 hr. **C**, Immunoblot analysis of TP53, p-RB and p-ATM and PARP cleavage and CC3 in ST8814 and S462.TY MPNST cells 24h after treatment with BCI (2 uM). **D**, ST8814 cells treated with BCI (2 uM) in combination with JNK-IN-8 (0–2.5 uM) and analyzed using the MTS assay. Experiments were done twice with n=6 per experiment. (*) and (**) represent $P<0.05$ and $P<0.01$.

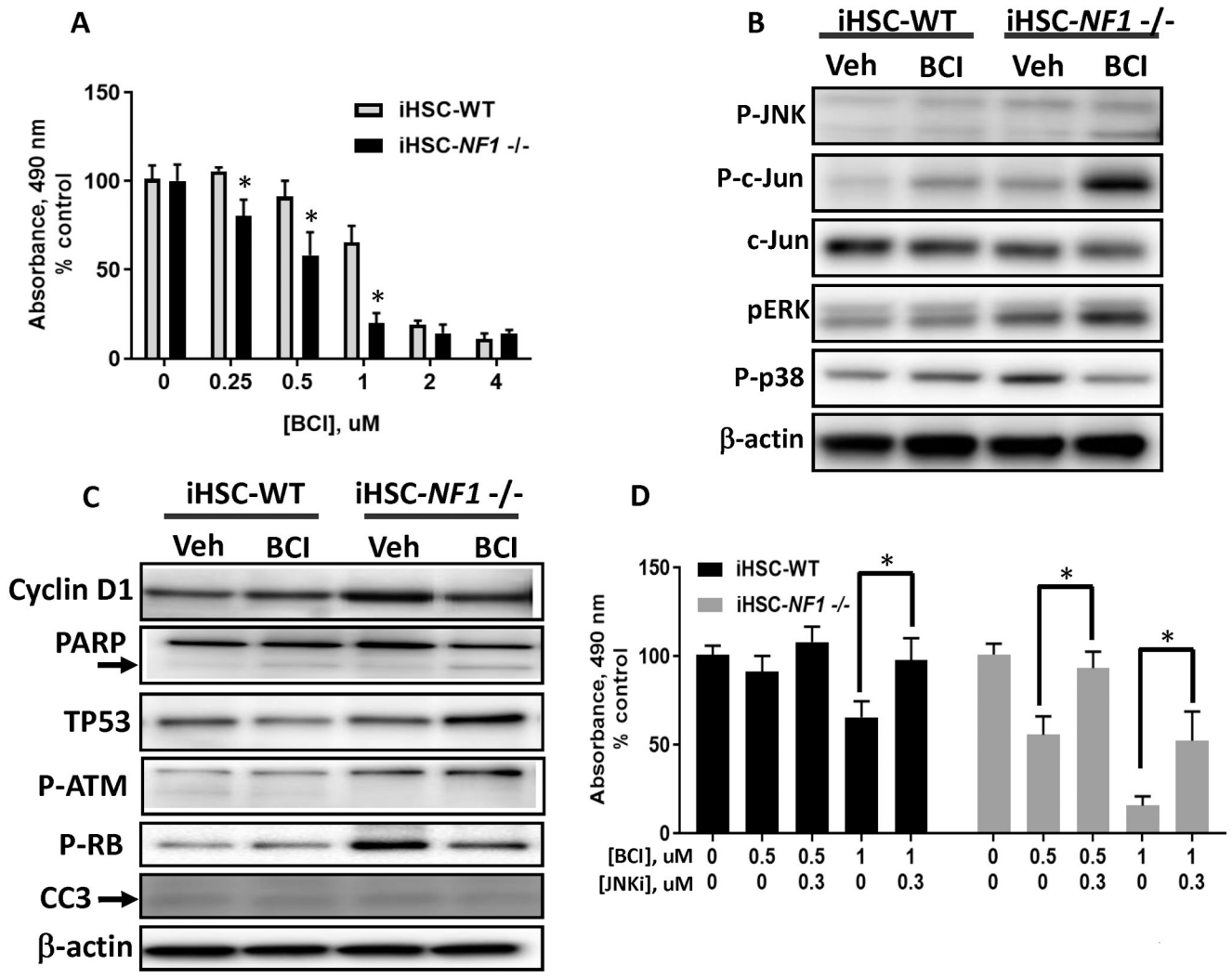

Figure 5.

NF1 loss increases efficacy of BCI treatment in Schwann cells. DUSP inhibition with BCI in immortalized human Schwann cells (iHSC) WT vs *NF1*-/−. **A**, Cell survival measured with the MTS assay. iHSC WT and *NF1*−/− cells were serum starved overnight and then treated with BCI (0–4 uM) in DMEM-F12 with N2 supplements and 10 ng/mL B-Heregulin (B-HRG) for 3 days. **B**, Immunoblot analysis of MAPK signaling after cells were starved overnight, pre-incubated with BCI (1 uM) for 60 mins then stimulated for 1 hr. **C**, Immunoblot analysis of cyclin D1, TP53, p-RB, p-ATM and PARP and CC3 in WT and *NF1*−/− iHSC after 24 h treatment with BCI (1 uM). **D**, Cell survival was measured with the MTS assay. Cells treated with BCI (0.5–1 uM), in combination with JNK-IN-8 (0.3 uM) for 3 days. (*) represents P<0.05. Experiments were done twice with n=4–6 per experiment.

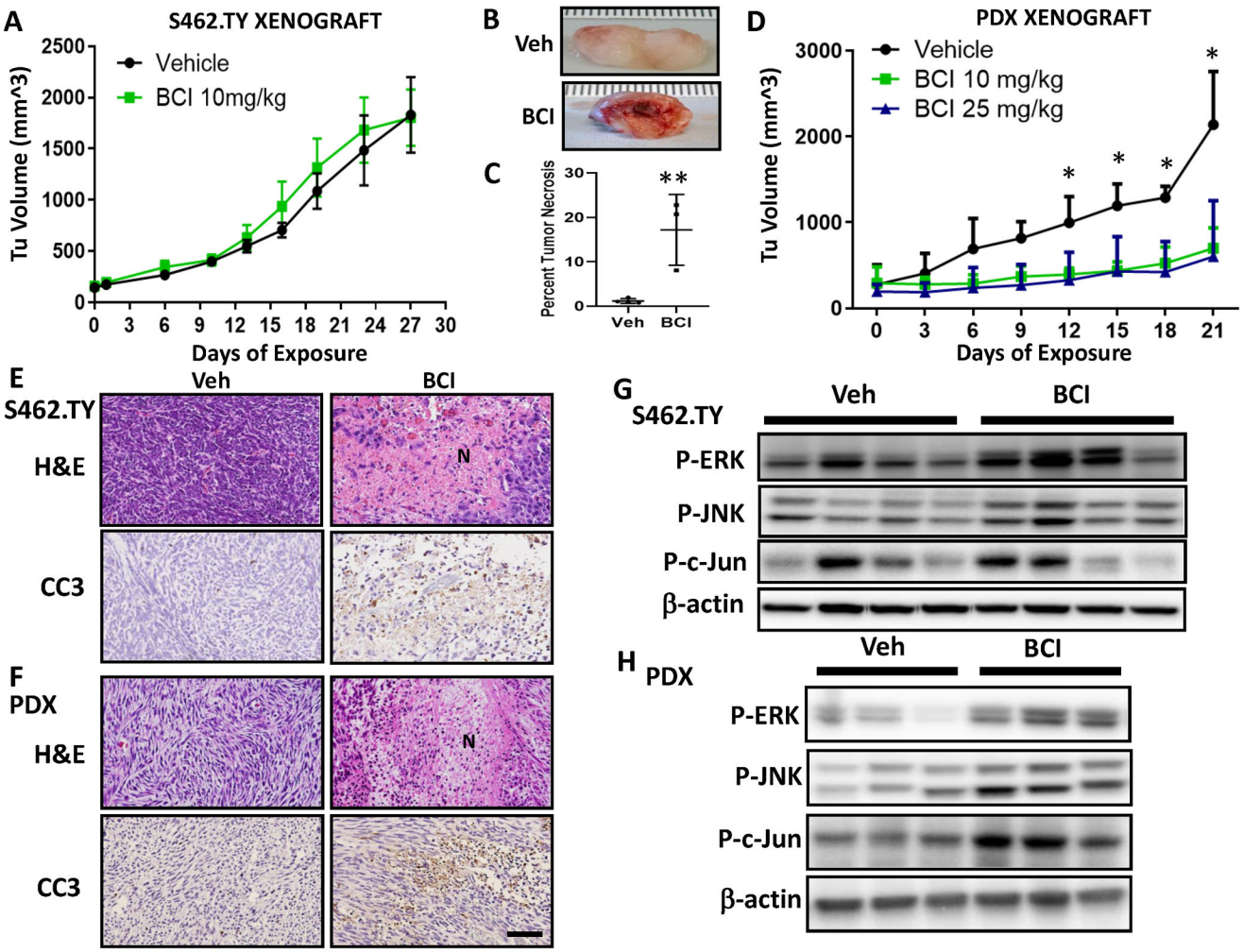

Figure 6.

In vivo DUSP inhibition causes tumor necrosis in MPNST xenograft models. **A**, Tumor volume (mm^3) in the S462.TY cell-based xenograft MPNST model dosed with vehicle (Veh) or BCI 10 mg/kg, i.p. once daily, 5x/wk for 27 days (n = 9) versus vehicle (n = 6). By day 27, mice required sacrifice. Data points represents mean +/− SEM. **B**, Gross image of S462.TY tumors with necrotic tissue (BCI treated) compared to vehicle-treated tumors. **C**, Quantification of tumor necrosis in the S462.TY xenograft MPNST model, expressed as percent total section area. Data points represents mean +/− SD. (**, $P < 0.01$, *t*-test). **D**, Tumor volume (mm^3) in the PDX-based xenograft MPNST model dosed with BCI (10 mg/kg or 25 mg/kg) i.p. once daily, 5x/wk for 21 days versus control (n = 5 per group). Data points represent mean +/− SEM. (*, $P < 0.05$, ANOVA, Tukey post-hoc test). **E**, Representative images of hematoxylin and eosin (H&E) stained and cleaved caspase-3 (CC3)-stained tissue sections in the S462.TY xenograft and **F**, PDX xenograft. Extensive necrosis (N) and increased CC3 occur compared to vehicle-treated tumors. Scale bar, 100 um. **G**, Immunoblot analysis of MAPK signaling markers in S462.TY xenograft model. Mice were dosed with BCI 10 mg/kg, i.p. once daily, 5x/wk for 27 days or vehicle and were sacrificed 2 hours after the last dose. **H**, Immunoblot analysis of MAPK signaling markers in

PDX MPNST tumors. Mice were dosed with BCI 10 mg/kg, i.p. once daily, 5x/wk for 12 days or vehicle and were sacrificed 2 hours after the last dose.